An Automatic Graph-Based Approach for Artery/Vein Classification in Retinal Images

Behdad Dashtbozorg, Ana Maria Mendonça, *Senior Member, IEEE*, and Aurélio Campilho, *Member, IEEE*

Abstract—The classification of retinal vessels into artery/vein (A/V) is an important phase for automating the detection of vascular changes, and for the calculation of characteristic signs associated with several systemic diseases such as diabetes, hypertension, and other cardiovascular conditions. This paper presents an automatic approach for A/V classification based on the analysis of a graph extracted from the retinal vasculature. The proposed method classifies the entire vascular tree deciding on the type of each intersection point (graph nodes) and assigning one of two labels to each vessel segment (graph links). Final classification of a vessel segment as A/V is performed through the combination of the graph-based labeling results with a set of intensity features. The results of this proposed method are compared with manual labeling for three public databases. Accuracy values of 88.3%, 87.4%, and 89.8% are obtained for the images of the INSPIRE-AVR, DRIVE, and VICAVR databases, respectively. These results demonstrate that our method outperforms recent approaches for A/V classification.

Index Terms—Artery/vein classification, graph, retinal images, vessel segmentation.

I. INTRODUCTION

A UTOMATED detection of retinopathy in eye fundus images using digital image analysis methods has huge potential benefits, allowing the examination of a large number of images in less time, with lower cost and reduced subjectivity than current observer-based techniques. Another advantage is the possibility to perform automated screening for pathological conditions, such as diabetic retinopathy, in order to reduce the workload required of trained manual graders [1].

Retinal vessels are affected by several systemic diseases, namely diabetes, hypertension, and vascular disorders. In diabetic retinopathy, the blood vessels often show abnormalities at early stages [2], as well as vessel diameter alterations [3]. Changes in retinal blood vessels, such as significant dilatation and elongation of main arteries, veins, and their branches [3], [4], are also frequently associated with hypertension and other cardiovascular pathologies.

Several characteristic signs associated with vascular changes are measured, aiming at assessing the stage and severity of some retinal conditions. Generalized arteriolar narrowing, which is inversely related to higher blood pressure levels [5], [6], is usually expressed by the Arteriolar-to-Venular diameter Ratio (AVR). The Atherosclerosis Risk in Communities (ARIC) study previously showed that a smaller retinal AVR might be an independent predictor of incident stroke in middle-aged individuals [7]. The AVR value can also be an indicator of other diseases, like diabetic retinopathy and retinopathy of prematurity [8]. Among other image processing operations, the estimation of AVR requires vessel segmentation, accurate vessel width measurement, and artery/vein (A/V) classification [9], [10]. Therefore, any automatic AVR measurement system must accurately identify which vessels are arteries and which are veins, since slight classification errors can have a large influence on the final value.

Several works on vessel classification have been proposed [11]–[17], but automated classification of retinal vessels into arteries and veins has received limited attention, and is still an open task in the retinal image analysis field. In recent years, graphs have emerged as a unified representation for image analysis, and graph-based methods have been used for retinal vessel segmentation [18], retinal image registration [19], and retinal vessel classification [12]. In this paper we propose a graph-based method for automatic A/V classification. The graph extracted from the segmented retinal vasculature is analyzed to decide on the type of intersection points (graph nodes), and afterwards one of two labels is assigned to each vessel segment (graph links). Finally, intensity features of the vessel segments are measured for assigning the final artery/vein class.

This paper is organized as follows. In Section II, some of the methods previously presented for retinal vessel classification are briefly reviewed. Section III presents the proposed graph-based approach for A/V classification. The results of tests on the images of three different databases are presented in Section IV, where a comparison with the manual classifications is also included. Finally, Section V summarizes the conclusions of the research.

II. METHODS FOR A/V CLASSIFICATION

There are visual and geometrical features that enable discrimination between veins and arteries; several methods have explored these properties for A/V classification [11]–[17]. Arteries are bright red while veins are darker, and in general

artery calibers are smaller than vein calibers. Vessel calibers can be affected by diseases, therefore this is not a reliable feature for A/V classification. Arteries also have thicker walls, which reflect the light as a shiny central reflex strip [20]. Another characteristic of the retinal vessel tree is that, at least in the region near the optic disc (OD), veins rarely cross veins and arteries rarely cross arteries, but both types can bifurcate to narrower vessels, and veins and arteries can cross each other [20]. For this reason, tracking of arteries and veins in the vascular tree is possible, and has been used in some methods to analyze the vessel tree and classify the vessels [11], [12].

A semi-automatic method for analyzing retinal vascular trees was proposed by Martinez-Perez *et al.* in [11]. In this method geometrical and topological properties of single vessel segments and subtrees are calculated. First, the skeleton is extracted from the segmentation result, and significant points are detected. For the labeling, the user should point to the root segment of the tree to be tracked, and the algorithm will search for its unique terminal points and in the end, decide if the segment is artery or vein. Another method similar to this was proposed by Rothaus *et al.* [12], which describes a rule-based algorithm to propagate the vessel labels as either artery or vein throughout the vascular tree. This method uses existing vessel segmentation results, and some manually-labeled starting vessel segments.

Grisan *et al.* [13] developed a tracking A/V classification technique that classifies the vessels only in a well-defined concentric zone around the optic disc. Then, by using the vessel structure reconstructed by tracking, the classification is propagated outside this zone, where little or no information is available to discriminate arteries from veins. This algorithm is not designed to consider the vessels in the zone all together, but rather partitions the zone into four quadrants, and works separately and locally on each of them.

Vazquez *et al.* [14] described a method which combines a color-based clustering algorithm with a vessel tracking method. First the clustering approach divides the retinal image into four quadrants, then it classifies separately the vessels detected in each quadrant, and finally it combines the results. Then, a tracking strategy based on a minimal path approach is applied to join the vessel segments located at different radii in order to support the classification by voting.

A piecewise Gaussian model to describe the intensity distribution of vessel profiles has been proposed by Li *et al.* [15]. In this model, the central reflex has been considered. A minimum distance classifier based on the Mahalanobis distance was used to differentiate between the vessel types using features derived from the estimated parameters.

Kondermann *et al.* [16] described two feature extraction methods and two classification methods, based on support vector machines and neural networks, to classify retinal vessels. One of the feature extraction methods is profile-based, while the other is based on the definition of a region of interest (ROI) around each centerline point. To reduce the dimensionality of the feature vectors, they used a multiclass principal component analysis (PCA).

Niemeijer *et al.* [17] proposed an automatic method for classifying retinal vessels into arteries and veins using image
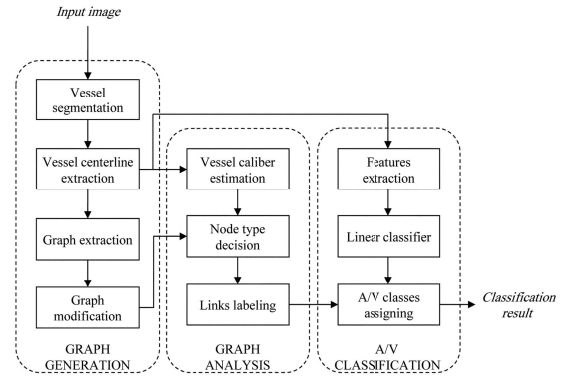

Fig. 1. Block diagram of the proposed method for A/V classification.

features and a classifier. A set of centerline features is extracted and a soft label is assigned to each centerline, indicating the likelihood of its being a vein pixel. Then the average of the soft labels of connected centerline pixels is assigned to each centerline pixel. They tested different classifiers and found that the *k*-nearest neighbor (kNN) classifier provides the best overall performance. In [21], the classification method was enhanced as a step in calculating the AVR value.

Most of these methods use intensity features to discriminate between arteries and veins. Due to the acquisition process, very often the retinal images are non-uniformly illuminated and exhibit local luminosity and contrast variability, which can affect the performance of intensity-based A/V classification methods. For this reason, we propose a method which uses additional structural information extracted from a graph representation of the vascular network. The results of the proposed method show improvements in overcoming the common variations in contrast inherent to retinal images.

III. GRAPH-BASED A/V CLASSIFICATION METHOD

The method proposed in this paper follows a graph-based approach, where we mostly focus on a characteristic of the retinal vessel tree that, at least in the region near the optic disc, veins rarely cross veins and arteries rarely cross arteries. Based on this assumption we may define different types of intersection points: bifurcation, crossing, meeting, and connecting points. A bifurcation point is an intersection point where a vessel bifurcates to narrower parts. In a crossing point a vein and an artery cross each other. In a meeting point the two types of vessels meet each other without crossing, while a connecting point connects different parts of the same vessel. The decision on the type of the intersection points are made based on the geometrical analysis of the graph representation of the vascular structure.

Fig. 1 depicts the block diagram of the proposed method for A/V classification. The main phases are: 1) graph generation; 2) graph analysis; and 3) vessel classification. The method first extracts a graph from the vascular tree, and afterwards makes a decision on the type of each intersection point (graph node). Based on the node types in each separate subgraph, all vessel segments (graph links) that belong to a particular vessel are identified and then labeled using two distinct labels. Finally, the A/V classes are assigned to the subgraph labels
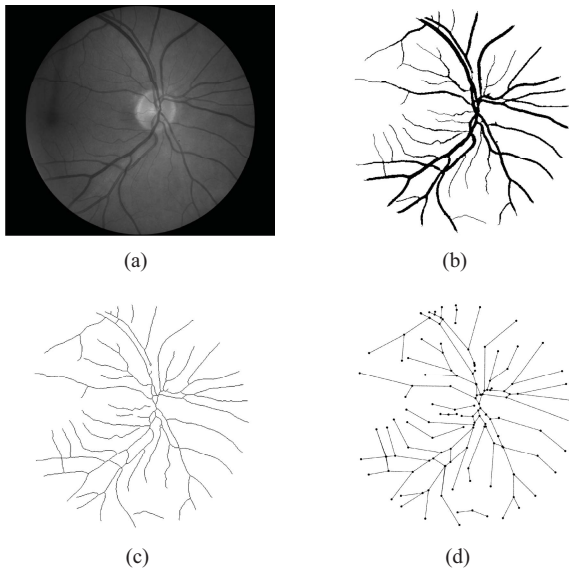
(a)   (b)

(c)   (d)

Fig. 2. Graph generation. (a) Original image; (b) Vessel segmentation image; (c) Centerline image; (d) Extracted graph.

TABLE I
GRAPH NOTATIONS

Notation	Description
N	Number of nodes in the graph
n_i, $\quad 1 \leq i < N$	Node i
D_{n_i}	Degree of node i
l_{ip}, $\quad 1 \leq p < D_{n_i}$	p^{th} link of node i
d_{ij}	Distance between node i and j
T_{n_i}	Type of node i
$\angle l_{ip} l_{iq}$	Angle between p^{th} and q^{th} links of node i
$W_{l_{ip}}$	Vessel caliber assigned to p^{th} link of node i
E_{n_i}	Number of degree 1 nodes adjacent to node i

by extracting a set of features and using a linear classifier. In the following we detail each phase of the proposed method.

A. Graph Generation

A graph is a representation of the vascular network, where each node denotes an intersection point in the vascular tree, and each link corresponds to a vessel segment between two intersection points. For generating the graph, we have used a three-step algorithm. First we use the segmented image to obtain the vessel centerlines, then the graph is generated from the centerline image, and finally some additional modifications are applied to the graph.

1) Vessel Segmentation: The vessel segmentation result is used for extracting the graph and also for estimating vessel calibers. The method proposed by Mendonça *et al.* [22] was used for segmenting the retinal vasculature, after being adapted for the segmentation of high resolution images [23].

This method follows a pixel processing-based approach with three phases. The first one is the pre-processing phase, where the intensity is normalized by subtracting an estimation of the image background, obtained by filtering with a large arithmetic mean kernel. In the next phase, centerline candidates are detected using information provided from a set of four directional Difference of Offset Gaussian filters, then connected into segments by a region growing process, and finally these segments are validated based on their intensity and length characteristics. The third phase is vessel segmentation, where multiscale morphological vessel enhancement and reconstruction approaches are followed to generate binary maps of the vessels at four scales. The final image with the segmented vessels is obtained by iteratively combining the centerline image with the set of images that resulted from the vessel reconstruction. Fig. 2(b) illustrates the result of vessel segmentation.

This method achieved an accuracy of 94.66% for the images of the DRIVE database, with an overall sensitivity and specificity of 0.75 and 0.98, respectively [23].

2) Vessel Centerline Extraction: The centerline image is obtained by applying an iterative thinning algorithm described in [24] to the vessel segmentation result. This algorithm removes border pixels until the object shrinks to a minimally connected stroke. The vessel centerlines from the segmented image of Fig. 2(b) are shown in Fig. 2(c).

3) Graph Extraction: In the next step, the graph nodes are extracted from the centerline image by finding the intersection points (pixels with more than two neighbors) and the endpoints or terminal points (pixels with just one neighbor). In order to find the links between nodes (vessel segments), all the intersection points and their neighbors are removed from the centerline image and as result we get an image with separate components which are the vessel segments. Next, each vessel segment is represented by a link between two nodes. Fig. 2(d) shows the graph obtained from the centerline image of Fig. 2(c).

The graph contains nodes, and at each node several links can be connected. On the other hand, any given link can only connect two nodes. Table I shows the graph notations for nodes and links which will be used in the rest of this document. The degree of a node is the number of adjacent nodes. Two nodes in a graph are called adjacent if they are connected by one link. The angle between links is defined as the magnitude of the smallest rotation that projects one of the links onto the other by considering the common node between them as the vertex. A vessel caliber is assigned to each link, as the average of the calibers along the corresponding vessel segment.

4) Graph Modification: The extracted graph may include some misrepresentation of the vascular structure as a result of the segmentation and centerline extraction processes. As defined in [12], the typical errors are (1) the splitting of one node into two nodes; (2) missing a link on one side of a node; (3) false link. The extracted graph should be modified when one of these errors is identified.

Node splitting: When extracting the centerline pixels in a single intersection, we have two graph nodes instead of only one. This situation, illustrated in Fig. 3(a), creates false nodes which affect the correctness of the final result of the graph analysis phase.

For addressing this problem we define an adaptive parameter, the threshold T_{ns}, which is used as the criterion for merging two neighborhood nodes. T_{ns} depends on the local
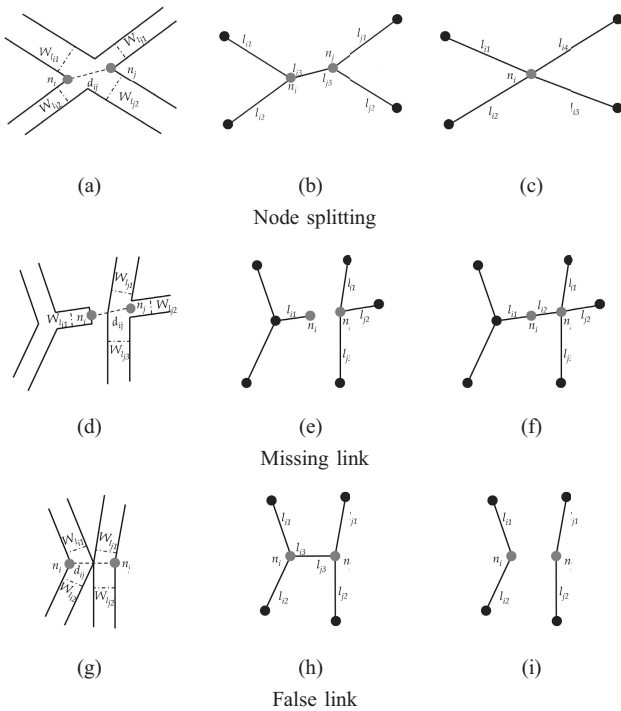
Fig. 3. Graph Modifications. (a), (d), (g) Typical errors; (b), (e), (e) Graph representation of the worst-case scenarios; (c), (f), (i) Final graph after modification.

vessel calibers and angles according to equations (1) to (4).

$$T_{ns} = \frac{1}{\sin(\alpha)} \left(d_1{}^2 + d_2{}^2 + 2d_1 d_2 \cos(\alpha) \right)^{1/2} \quad (1)$$

$$\alpha = \min\left(\angle l_{i1} l_{i2}, \angle l_{j1} l_{j2}\right) \quad (2)$$

$$d_1 = \max\left(W_{l_{i1}}, W_{l_{j2}}\right) \quad (3)$$

$$d_2 = \max\left(W_{l_{i2}}, W_{l_{j1}}\right). \quad (4)$$

In adjacent nodes with degree 3, Fig. 3(b), if the distance between node n_i and n_j is smaller than the threshold ($d_{ij} < T_{ns}$) and if a link in one node (common link excluded) has the same orientation of another link in the other node, and the same happens with the two remaining links, then the two corresponding nodes should be merged (Fig. 3(c)).

Missing link: For solving the missing link cases (Fig. 3(d)), the distance from a degree 1 node (endpoints) to other nodes is calculated. If this distance is less than a threshold T_{ml}, then the nodes will be connected with a new link as shown in Fig. 3(f). T_{ml} estimation is based on the widths of the intervening vessels (Fig. 3(e)), and is given by

$$T_{ml} = W_{l_{i1}} + \max_{p \in \{1,2,3\}} W_{l_{jp}}. \quad (5)$$

False link: Fig. 3(g) illustrates the last situation, corresponding to an incorrect detection of a link between two nodes. This happens when two vessels are very close to each other but they do not cross, and two close nodes ($d_{ij} < T_{fl}$) are artificially created. Equation (6) represents the threshold T_{fl} for this case, which is obtained from the maximum distance of nodes in the

---

Algorithm 1 Graph Modification

for $i = 1$ to N **do**
  for $j = 1$ to N, $j \neq i$ **do**
    if $D_{n_i} = 1 \land d_{ij} < T_{ml}$ **then**
      Make a new link (l_{i2}) between n_i, n_j
    else if n_i, n_j are adjacent $\land D_{n_i} = 3 \land D_{n_j} = 3$ **then**
      if $d_{ij} < T_{sn} \land (\angle l_{i1} l_{i3} + \angle l_{j2} l_{j3} = 180° \pm 10°) \land (\angle l_{i2} l_{i3} + \angle l_{j1} l_{j3} = 180° \pm 10°)$ **then**
        Merge n_i and n_j
      else if $d_{ij} < T_{fl} \land ((\angle l_{i1} l_{i3} = 90° \pm 5° \land \angle l_{i2} l_{i3} = 90° \pm 5°) \lor (\angle l_{j1} l_{j3} = 90° \pm 5° \land \angle l_{j2} l_{j3} = 90° \pm 5°))$ **then**
        Remove the link between n_i, n_j (l_{i3}, l_{j3})
      end if
    end if
  end for
end for

---

worst-case scenario (Fig. 3(h)).

$$T_{fl} = \max_{p \in \{1,2\}} \left(\frac{W_{l_{ip}}}{\sin\left(\angle l_{ip} l_{i3}\right)} \right) + \max_{q \in \{1,2\}} \left(\frac{W_{l_{jq}}}{\sin\left(\angle l_{jq} l_{j3}\right)} \right). \quad (6)$$

For solving this case, the angle between the links connected to each node is checked. If, for at least one node, two of its links have an identical orientation and are more or less perpendicular to the third link (the common link between two nodes), then the common link is a falsely-detected link and should be removed (Fig. 3(i)).

Algorithm 1 states the conditions for detecting errors in the graph and for performing the necessary modifications. This algorithm repeats until no further changes occur. In order to reduce the complexity of the subsequent graph analysis, all endpoints with very short links are removed.

Before initiating the graph analysis phase, all vessels around the OD are removed. The optic disc area usually contains many vessels and the graph in that area is not reliable. As these vessels are not relevant for the A/V classification process, they can be removed. The result is a graph formed by several non-connected separate subgraphs. The operations in the graph modification step are illustrated in Fig. 4.

B. Graph Analysis

The output of the graph analysis phase is a decision on the type of the nodes. The links in each subgraph (i) are labeled with one of two distinct labels (C_1^i and C_2^i). In this phase we are not yet able to determine whether each label corresponds to an artery class or to a vein class. The A/V classes will be assigned to these subgraphs only in the last classification phase.

We have considered four different types of nodes:

1. Connecting point: most of the nodes with two links belong to this type; these nodes, where vessels never cross or bifurcate, are continuation nodes connecting different segments of the same vessel.

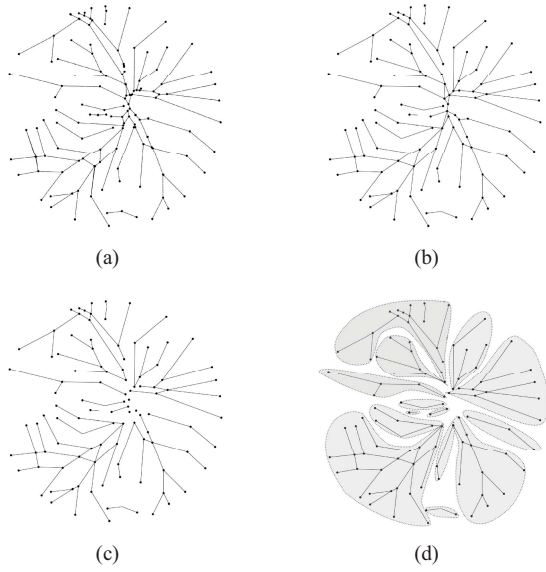2. Crossing point: two different types of vessels cross each other.

Fig. 4. (a) Original graph; (b) New graph after modification step; (c) Modified graph without vessels around the optic disc; (d) Separate subgraphs (each gray region represents a subgraph).

Fig. 5. (a)–(c) Possible configurations for nodes of degree 2; (d)–(f) Possible configurations for nodes of degree 3.

TABLE II
DIFFERENT CASES OF NODES AND THE POSSIBLE NODE TYPES

Cases	Possible Node Types
Case 1 - Nodes of degree 2	Connecting point
	Meeting point
Case 2 - Nodes of degree 3	Bifurcation point
	Meeting point
Case 3 - Nodes of degree 4	Bifurcation point
	Meeting point
	Crossing point
Case 4 - Nodes of degree 5	Crossing point

Fig. 6. (a)–(c) Possible configurations for nodes of degree 4; (d) Node of degree 5.

3. Bifurcation point: a vessel bifurcates into narrower vessels.

4. Meeting point: two different types of vessels meet each other without crossing; the two vessels are very close to each other or one vessel ends exactly on the other vessel.

The node classification algorithm starts by extracting the following node information: the number of links connected to each node (node degree), the orientation of each link, the angles between the links, the vessel caliber at each link, and the degree of adjacent nodes.

Node analysis is divided into four different cases depending on the node degree. Table II shows the different cases, and the possible node types for each. In Figs. 5 and 6, the nodes under analysis are represented by gray dots and other nodes are represented as black dots, except the endpoints which are represented as white dots. Solid lines show the links for one label and the dashed lines represent the other label.

1) Nodes of Degree 2: Nodes with two links are mostly connecting nodes. If at least one of its adjacent nodes is an endpoint, then the node is a connecting point (Fig. 5(a)) and both links have the same label; however, if none of the adjacent nodes are endpoints then the node type depends on the angle
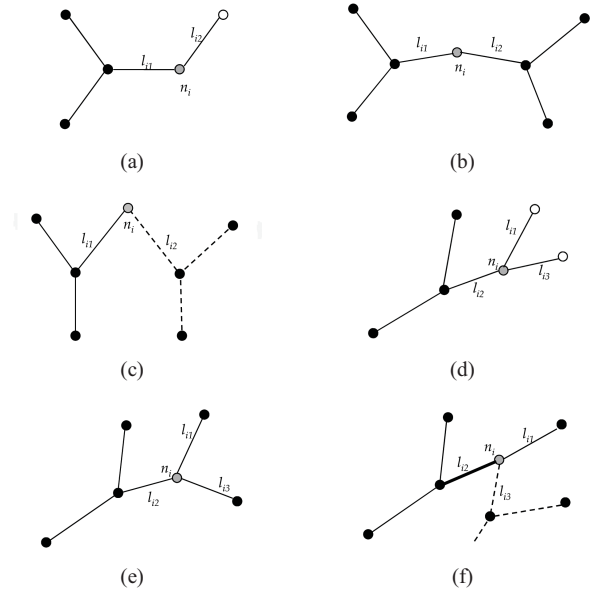

Algorithm 2 Node type- Nodes of degree 2

> **for** $i = 1$ to N **do**
>> **if** $D_{n_i} = 2$ **then**
>>> **if** $E_{n_i} \geq 1$ **then**
>>>> $T_{n_i} =$ Connecting point
>>>
>>> **else if** $\angle l_{i1} l_{i2} \leq 90°$ **then**
>>>> $T_{n_i} =$ Meeting point
>>>
>>> **else**
>>>> $T_{n_i} =$ Connecting point
>>>
>>> **end if**
>>
>> **end if**
>
> **end for**

---

between its links. If $\angle l_{i1} l_{i2} > 90°$ then it is a connecting node (Fig. 5(b)), otherwise it is a meeting point and the links have different labels (Fig. 5(c)). Algorithm 2 details the procedure for deciding on the type of nodes of degree 2.

Algorithm 3 Node type- Nodes of degree 3

---

for $i = 1$ to N **do**
  if $D_{n_i} = 3$ **then**
    if $E_{n_i} \geq 2$ **then**
      $T_{n_i} =$ Bifurcation point
    else
      $flag = 0$
      for $p, q, r = 1$ to 3 **do**
        if $\angle l_{ip} l_{iq} = 180° \pm 10° \wedge flag = 0$ **then**
          $flag = 1$
          if $W_{l_{ip}} > W_{l_{iq}} \wedge \angle l_{ip} l_{ir} < 90°$ **then**
            $T_{n_i} =$ Meeting point
          else
            $T_{n_i} =$ Bifurcation point
          end if
        end if
      end for
      if $flag = 0$ **then**
        $T_{n_i} =$ Bifurcation point
      end if
    end if
  end if
end for

Algorithm 4 Node type- Nodes of degree 4

---

for $i = 1$ to N **do**
  if $D_{n_i} = 4$ **then**
    for $p, q, r, s = 1$ to 4 **do**
      if $\angle l_{ip} l_{iq} = 180° \pm 10° \wedge \angle l_{ir} l_{is} = 180° \pm 10°$ **then**
        $T_{n_i} =$ Crossing point
      else if $\angle l_{ip} l_{iq} = 180° \pm 10° \wedge W_{l_{ip}} < W_{l_{iq}} \wedge \angle l_{ip} l_{ir} <$
$90° \wedge \angle l_{ip} l_{is} < 90°$ **then**
        $T_{n_i} =$ Bifurcation point
      else
        $T_{n_i} =$ Meeting point
      end if
    end for
  end if
end for

---

2) Nodes of Degree 3: For each node with 3 links, if at least two adjacent nodes are endpoints then the node is a bifurcation point and all the links have the same label (Fig. 5(d)). If all the connected links have different orientations then the node is also a bifurcation point (Fig. 5(e)). If two links have the same orientation then both belong to the same vessel type (Fig. 5(f)) and they will be considered as a main vessel. We can decide if the third link is a branch of the same vessel or a segment of another vessel by checking its angle with the thicker segment of the main vessel. The thicker segment of the main vessel can be found by comparing the vessel caliber assigned to each link. If the difference between vessel calibers is very small, then it is not reliable to find the thicker one based on the calibers; in this situation, the link connected to the closest node to the optic disc center represents the thicker segment of the main vessel, and the link connected to the farthest node is the thinner segment of the main vessel. If the third link makes an angle less than 90° with the thicker segment of the main vessel then it is not a branch of this vessel but a part of another vessel, and the node is a meeting point; otherwise, it is a branch and all links have the same label. The sequence of operations for finding the type of nodes of degree 3 is described in Algorithm 3.

3) Nodes of Degree 4: In this case there are three node type possibilities. First, the four links are grouped into two pairs, each one formed by the two links with the highest angle between them; if the two links of each of these pairs have an identical orientation (Fig. 6(a)), then the node is a crossing point and each pair of links has a different label.

If the links of one pair do not have the same orientation, then the other pair will be selected as the main vessel. If the angle between each one of the other links and the thinner part of the main vessel is less than 90°, then the node is considered a bifurcation point and all links have the same label (Fig. 6(b)). If one of these links makes an angle less than 90° with the thicker segment of the main vessel, then it has a different label and the node is a meeting point (Fig. 6(c)). Algorithm 4 details the procedure for finding the type for nodes of degree 4.

4) Nodes of Degree 5: This is a rare situation that happens when a vessel crosses another vessel on a bifurcation point. For labeling, we start by finding the two links with the largest angle between them, as for instance l_{i3} and l_{i5} in Fig. 6(d). These links belong to the vessel which crosses the other vessel on its bifurcation point, so these links will have the same label. The other three links (l_{i1}, l_{i2} and l_{i4}) belong to the vessel which bifurcates in this node, therefore all these links will be marked with the other label.

After deciding on the node types, all links that belong to a particular vessel are identified and labeled. The final result is the assignment of two labels in each separate subgraph. This means that labels C_1^1, C_2^1 will be assigned to the links in subgraph 1, labels C_1^2, C_2^2 to the links in subgraph 2 and so on.

The link labeling process starts by locating the optic disc center (ODC) using the automatic method based on the entropy of vascular directions, proposed by Mendonça *et al.* [25]. Then for each separate subgraph, the farthest link from the ODC is detected, and a label is assigned to this link (for instance C_1^1); the node connected to this link is found, and based on the node type the other links are labeled as C_1^1 or C_2^1. This procedure is repeated for all nodes until there are no more links for each subgraph. After finishing the labeling of one separate subgraph, we will repeat the process for all the separate subgraphs, each time defining two new labels, until the entire graph is processed. In the end we have a graph with different pairs of labels for each disjoint subgraph, as illustrated in Fig. 7(a), where each color in a separate subgraph represents a different label.

C. A/V Classification

The above described labeling phase used the vessel structural information embedded in the graph representation. Based
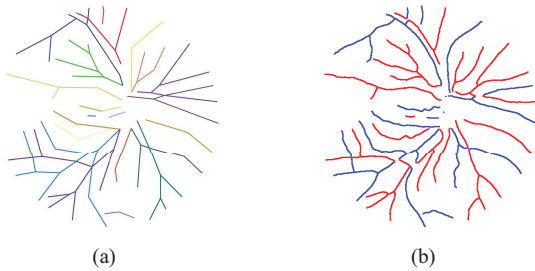
(a)   (b)

Fig. 7.   (a) Graph analysis result; (b) A/V classification result (Red: correctly classified arteries, Blue: correctly classified veins).

TABLE III

LIST OF FEATURES MEASURED FOR EACH CENTERLINE PIXEL

Nr.	Features
1-3	Red, Green and Blue intensities of the centerline pixels.
4-6	Hue, Saturation and Intensity of the centerline pixels.
7-9	Mean of Red, Green and Blue intensities in the vessel.
10-12	Mean of Hue, Saturation and Intensity in the vessel.
13-15	Standard deviation of Red, Green and Blue intensities in the vessel.
16-18	Standard deviation Hue, Saturation and Intensity in the vessel.
19-22	Maximum and minimum of Red and Green intensities in the vessel.
23-30	Intensity of the centerline pixel in a Gaussian blurred ($\sigma = 2, 4, 8, 16$) of Red and Green plane.

TABLE IV

PERFORMANCE EVALUATION AND COMPARISON OF INDIVIDUAL INTENSITY-BASED CLASSIFIERS (INSPIRE-AVR DATABASE)

Classifier	Selected Features	Most important feature	Accuracy-centerline pixels	Accuracy-labeling links
LDA	No. 1, 2, 7, 10, 12-14, 16, 17, 19, 20, 23-30	No. 1	75.2%	79.7%
QDA	No. 1-3, 7, 8, 13, 14, 19, 21-23	No. 1	73.2%	75.9%
kNN	No. 1-3, 7-9, 13,14, 16, 20, 23	No. 13	68.3%	73.0.%

on these labels, the final goal is now to assign the artery class (A) to one of the labels, and the vein class (V) to the other. For this purpose we add to the structural information, vessel intensity information in order to allow the final discrimination between A/V classes.

As a result of the acquisition process, very often the retinal images are non-uniformly illuminated and exhibit local luminosity and contrast variability. In order to make the classifier more robust, each image is processed using the method proposed by M. Foracchia *et al.* [26], which normalizes both luminosity and contrast based on a model of the observed image. Luminosity and contrast variability in the background are estimated and then used for normalizing the whole image.

For each centerline pixel, the 30 features listed in Table III are measured and normalized to zero mean and unit standard deviation. Some of these features were used previously in [13], [21]. We have tested the most commonly used classifiers, namely linear discriminant analysis (LDA), quadratic discriminant analysis (QDA), and *k*-nearest neighbor (kNN), on the INSPIRE-AVR dataset. For feature selection, we have used sequential forward floating selection, which starts with an empty feature set and adds or removes features when this improves the performance of the classifier.

Table IV shows the performance of intensity-based classifiers on the INSPIRE-AVR image database using 2-fold cross-validation. This table contains the accuracy values obtained when these classifiers are used for centerline pixel classification, and also for labeling vessel segments (links). The LDA classifier provided the best results and was selected for the A/V classification phase, using the set of selected features (1-2, 7, 10, 12-14, 16-17, 19-20 and 23-30).

The trained classifier is used for assigning the A/V classes to each one of the subgraph labels. First, each centerline pixel is classified into A or V classes, then for each label (C_j^i, $j = 1, 2$) in subgraph i, the probability of its being an artery is calculated based on the number of associated centerline pixels classified by LDA to be an artery or a vein. The probability of label C_j^i to be an artery is $P_a(C_j^i) = n_{C_j^i}^a / (n_{C_j^i}^a + n_{C_j^i}^v)$ where $n_{C_j^i}^a$ is the number of centerline pixels of a label classified as an artery and $n_{C_j^i}^v$ is the number of centerline pixels classified as a vein. For each pair of labels in each subgraph, the label with higher artery probability will be assigned as an artery class, and the other as a vein class.

Finally, to prevent a wrong classification as a result of a wrong graph analysis, we calculate the probability of being an artery or a vein for each link individually. The probability of a link (l_i) being an artery ($P_a(l_i)$) is computed as $P_v(l_i) = n_{l_i}^v / \left(n_{l_i}^a + n_{l_i}^v \right)$, and the probability of being a vein (($P_v(l_i)$)) is computed as $P_v(l_i) = n_{l_i}^v / \left(n_{l_i}^a + n_{l_i}^v \right)$, where $n_{l_i}^a$ is the number of centerline pixels of link (l_i) classified as an artery and $n_{l_i}^v$ is the number of centerline pixels classified as a vein. If the probability of being an artery is higher than 0.9 ($P_a(l_i) \geq 0.9$) then the link will be assigned as an artery, and if $P_v(l_i) \geq 0.9$ then it will be assigned as a vein, without considering the result of the graph analysis.

The result of assigning a class to the link centerline pixels is shown in Fig. 7(b). The red color represents arteries and blue color represents the veins.

IV. RESULTS

The automatic methods described in the previous sections were tested on the images of three databases, DRIVE [27], INSPIRE-AVR [28], and VICAVR [29]. The images in the DRIVE dataset were captured with 768×584 pixels, with 8 bits per color plane. The 40 high resolution images of the INSPIRE-AVR database have resolution of 2392×2048 pixels and are optic disc-centered. Finally, the 58 images of the VICAVR database were acquired using a TopCon non-mydriatic camera NW-100 model with a spatial resolution of 768×584, and are also optic disc-centered. Results of automatic vessel segmentation were available for the three datasets, and a manual artery/vein labeling was performed by an expert on the 20 images of the DRIVE test set and for the 40 images of the INSPIRE database. The VICAVR database includes the caliber of the vessels measured at different radii

TABLE V

ACCURACY OF INDIVIDUAL METHODS BEFORE AND AFTER
COMBINATION (INSPIRE-AVR DATABASE)

	Method	Centerline pixels in entire image	All vessel pixels in entire image	Centerline pixels inside ROI	All vessel pixels inside ROI
Semi-automatic	Manual assignment of A/V classes to the sub-graph labels	90.7%	92.3%	91.4%	93.7%
Automatic	LDA-only	79.9%	85.0%	80.4%	86.2%
	Combination of graph-based method with LDA	84.9%	88.3%	95.9%	91.1%

TABLE VI

ACCURACY RATES FOR THE ENTIRE IMAGE AND INSIDE THE ROI
(INSPIRE-AVR DATABASE)

Vessel Caliber (vc)	Centerline pixels in entire image	All vessel pixels in entire image	Centerline pixels inside ROI	All vessel pixels inside ROI
$vc > 0\ pixels$	84.9%	88.3%	85.9%	91.1%
$vc > 5\ pixels$	86.5%	88.7%	87.9%	91.4%
$vc > 10\ pixels$	89.6%	90.5%	91.1%	92.8%
$vc > 15\ pixels$	92.6%	92.8%	95.9%	96.2%
$vc > 20\ pixels$	93.4%	93.4%	97.1%	97.2%

TABLE VII

COMPARISON OF SENSITIVITY AND SPECIFICITY VALUES

Method	INSPIRE-AVR		DRIVE	
	Sensitivity	Specificity	Sensitivity	Specificity
Graph-based	0.91	0.86	0.90	0.84
Niemeijer (best cut-off[1])	≈0.78	≈0.78	≈0.80	≈0.80
Niemeijer (sensitivity cut-off)	≈0.91	≈0.63	≈0.90	≈0.67
Niemeijer (specificity cut-off)	≈0.60	≈0.86	≈0.73	≈0.84

[1] cut-off: specific point on the ROC curve for extracting sensitivity and specificity values

from the optic disc as well as the vessel type (artery/vein) labeled based on the agreement among three experts.

The following subsections present the results of applying the proposed A/V classification method on the images of these databases. The accuracy values are obtained for centerline and vessel pixels in the entire image, as well as for the pixels inside the region of interest (ROI) that is usually defined for the calculation of the arteriolar-to-venular ratio; the ROI is the standard ring area within 0.5 to 1.0 disc diameters from the optic disc margin [10].

A. INSPIRE-AVR Dataset

In the INSPIRE-AVR dataset, we have used 2-fold cross-validation. We randomly assigned images to two sets S_1 and S_2, so that both sets were of equal size. We then trained the classifier on S_1 and tested it on S_2, followed by training on S_2 and testing on S_1. For training the LDA classifier, we randomly selected 15,000 labeled centerline pixels from each set. Some results of the proposed A/V classification method on this database are shown in Fig. 8.

Table V shows the performance evaluation of the individual LDA classifier for classifying vessel segments in INSPIRE-AVR database, and the results obtained using the combination of graph-based classification with LDA. The analysis of these values shows that the graph-based method with LDA outperforms the accuracy of the LDA classifier alone. For further evaluation of the graph-based method, we consider a semi-automatic approach by manually assigning the A/V classes to the labels of each subgraph. The results obtained are included in the first row of Table V. The high accuracy of the semi-automatic approach is a good indication that the structural information embedded in the graph-based method is important *per se* for link labeling. This is confirmed by the superior results achieved by the combination of the graph-based and LDA methods, when compared with LDA-only.

For evaluating the proposed method, which is the combination of graph-based classification with LDA, we have calculated the accuracy both for centerline pixel classification and for vessel pixel classification. Table VI shows the accuracy values for centerline and vessel pixels in the entire image, as well as for the pixels inside the region of interest (ROI). Each row of Table VI contains the accuracy values calculated using

different ranges for vessel calibers. The first row contains the results for all the vessels, while the remaining rows present the results for vessels with caliber higher than 5, 10, 15 and 20 pixels.

We have also calculated the percentage of correctly classified vessel pixels of the six largest arteries and the six largest veins inside the ROI, as these are the vessels normally used for AVR calculation. An accuracy value of 98.0% was obtained, thus demonstrating that the proposed methodology for A/V classification is reliable for use in an automated procedure for AVR calculation.

Results for A/V classification in INSPIRE-AVR images were presented by Niemeijer *et al.* using a receiver operator characteristic (ROC) curve. The reported value for the area under the curve (AUC) was 0.84 for the vessel centerline pixels inside the ROI of INSPIRE-AVR images [21].

By considering arteries as negatives and veins as positives, we obtained the sensitivity value of our results by computing the proportion of positives which are correctly identified, while specificity is measured by the proportion of negatives which are correctly identified. To facilitate comparison with the results of our method, sensitivity and specificity values were extracted from the figure of ROC curve presented in [21], after selecting three specific cut-off points on the curve: 1) best cut-off (the balanced sensitivity and specificity values are extracted from the curve); 2) sensitivity cut-off (the specificity value is extracted from the curve on a point where the sensitivity value is identical to the result of our method); 3) specificity cut-off (the sensitivity value is extracted from the curve on a point where the specificity value is identical to the result of our method). The comparison of sensitivity and specificity values are presented in the second and third columns of Table VII.
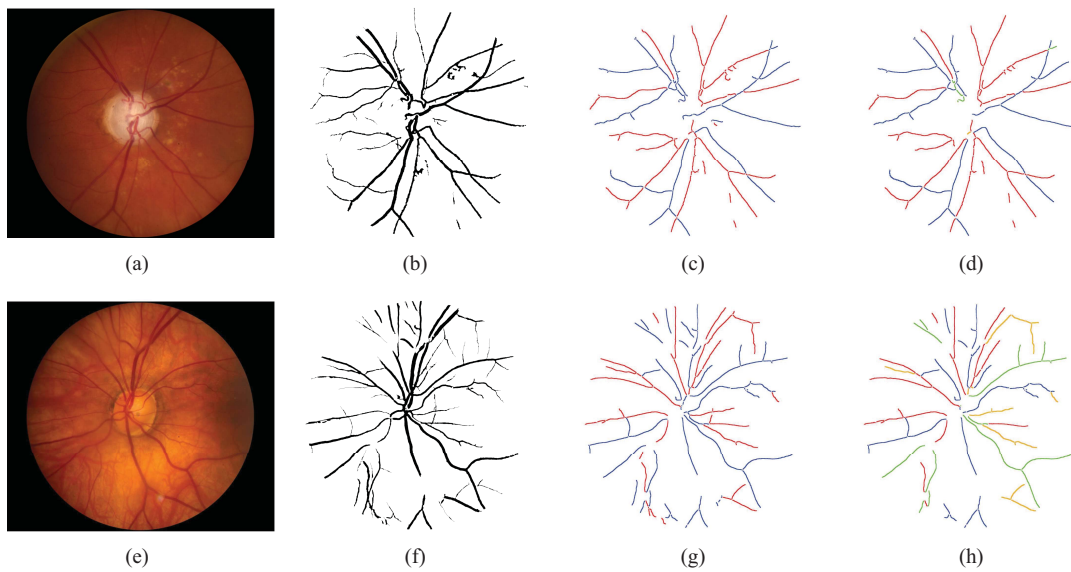
Fig. 8. Top row: best result for the INSPIRE-AVR database (accuracy = 97.7%). Bottom row: worst result for the INSPIRE-AVR database (accuracy = 61.2%). (a), (e) Original images; (b), (f) Segmentation results; (c), (g) A/V classification results; (d), (h) Comparisons with manual labeling (Red: correctly classified arteries, Blue: correctly classified veins, Green: wrongly classified arteries, Brown: wrongly classified veins).
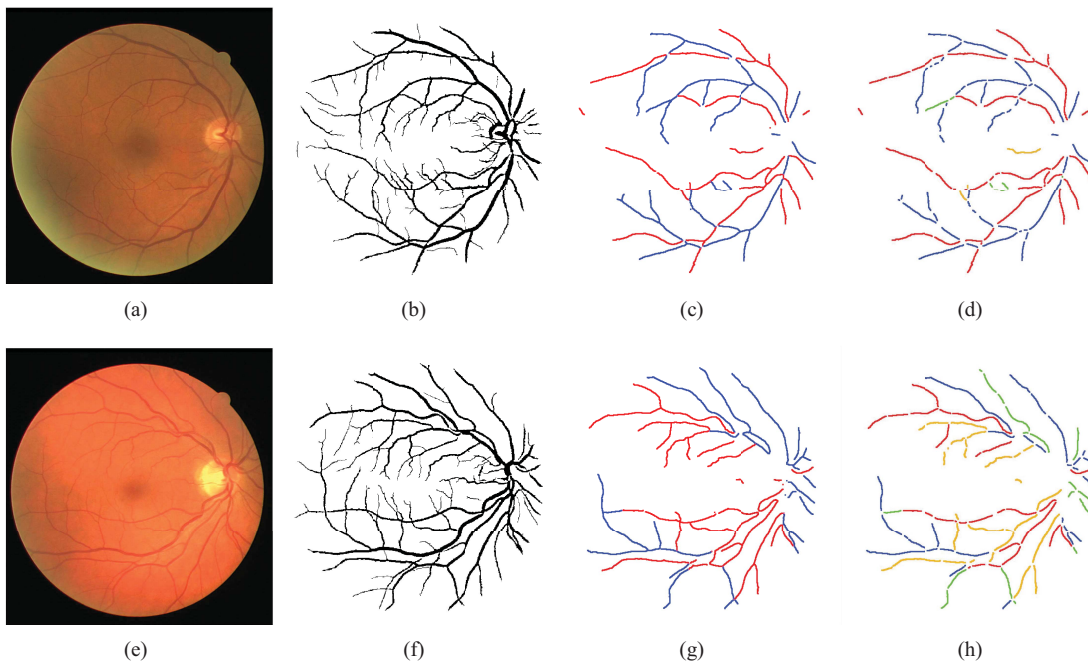

Fig. 9. Top row: best result for the DRIVE database (accuracy = 96.1%). Bottom row: worst result for the DRIVE database (accuracy = 72.9%). (a), (e) Original images; (b), (f) Segmentation results; (c), (g) A/V classification results; (d), (h) Comparisons with manual labeling (Red: correctly classified arteries, Blue: correctly classified veins, Green: wrongly classified arteries, Brown: wrongly classified veins).

B. DRIVE Dataset

For the 20 test images of the DRIVE database, an accuracy of 87.4% was achieved for the classification of centerline pixels of the main vessels (vessels with caliber higher than 3 pixels). Two examples of automatic classification of DRIVE images can be observed in Fig. 9. The differences between the results of the proposed method and manual labeling are shown in green (wrongly classified arteries) and yellow (wrongly classified veins), while the correctly classified arteries and veins are presented in red and blue, respectively.

Niemeijer *et al.* presented the results of their A/V classification method in DRIVE images using a ROC curve. The AUC value was 0.88 for the main vessel centerline pixels of DRIVE [17]. The sensitivity and specificity values were extracted from the figure of ROC curve presented in [17] on three cut-off points which are included in the two rightmost
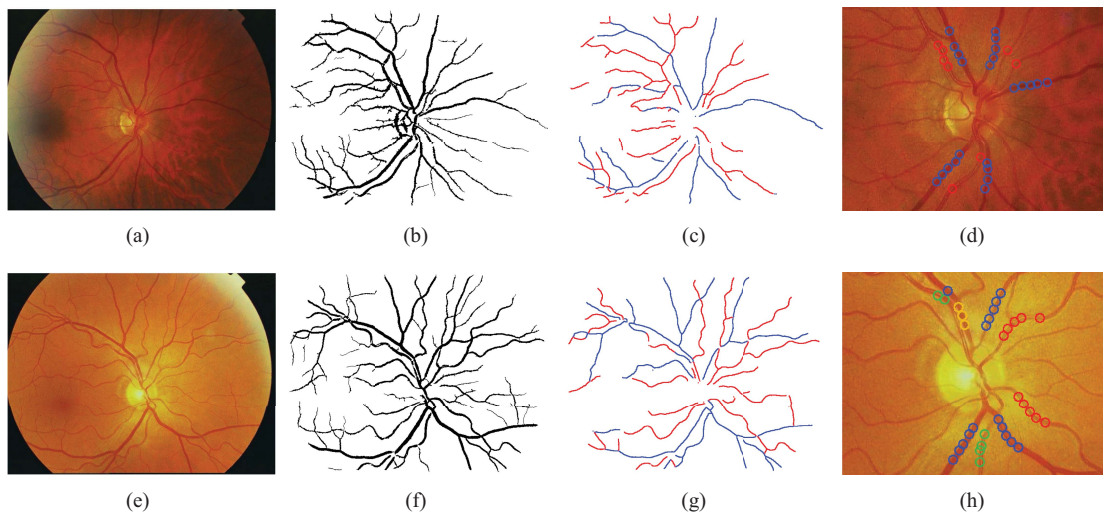
Fig. 10. Top row: best result for the VICAVR database (accuracy = 100%). Bottom row: worst result for the VICAVR database (accuracy = 74.3%). (a), (e) Original images; (b), (f) Segmentation results; (c), (g) A/V classification results; (d), (h) Comparisons with manual labeling (Red circle: correctly classified artery segments, Blue circle: correctly classified vein segments, Green circle: wrongly classified arteries, Brown circle: wrongly classified veins).

columns of Table VII. For all calculated values, our proposed graph-based classification method outperforms Niemeijer's approach.

C. VICAVR Dataset

For the 2116 vessel segments of VICAVR images that have manual classification results, the percentage of correctly-classified vessel segments using the graph-based solution is 89.8%, which is similar to the value achieved by Vazquez *et al.* (88.80%) [14]. Some results of the proposed A/V classification method on the images of VICAVR are shown in Fig. 10.

V. CONCLUSION

The classification of arteries and veins in retinal images is essential for the automated assessment of vascular changes. In previous sections, we have described a new automatic methodology to classify retinal vessels into arteries and veins which is distinct from prior solutions. One major difference is the fact that our method is able to classify the whole vascular tree and does not restrict the classification to specific regions of interest, normally around the optic disc. While most of the previous methods mainly use intensity features for discriminating between arteries and veins, our method uses additional information extracted from a graph which represents the vascular network.

The information about node degree, the orientation of each link, the angles between links, and the vessel caliber related to each link are used for analyzing the graph, and then decisions on type of nodes are made (bifurcation, crossing, or meeting points). Next, based on the node types, the links that belong to a particular vessel are detected, and finally A/V classes are assigned to each one of these vessels using a classifier supported by a set of intensity features.

The graph-based method with LDA outperforms the accuracy of the LDA classifier using intensity features, which shows the relevance of using structural information for A/V

classification. Furthermore, we compared the performance of our approach with other recently proposed methods, and we conclude that we are achieving better results.

The promising results of the proposed A/V classification method on the images of three different databases demonstrate the independence of this method in A/V classification of retinal images with different properties, such as differences in size, quality, and camera angle. On the other hand, the high accuracy achieved by our method, especially for the largest arteries and veins, confirm that this A/V classification methodology is reliable for the calculation of several characteristic signs associated with vascular alterations. Further research is planned using the graph that represents the vessel tree and the A/V classification method for AVR calculation, as well as identifying other vascular signs, such as vascular bifurcation angles, branching patterns, and fractal-based features, which can have significant impact on the early detection and follow-up of diseases, namely diabetes, hypertension, and cardiovascular diseases.

ACKNOWLEDGMENT

REFERENCES

[1] N. Patton, T. M. Aslam, T. MacGillivray, I. J. Deary, B. Dhillon, R. H. Eikelboom, K. Yogesa, and I. J. Constable, "Retinal image analysis: Concepts, applications and potential," *Progr. Retinal Eye Res.*, vol. 25, p. 99–127, Jan. 2006.

[2] T. T. Nguyen and T. Y. Wong, "Retinal vascular changes and diabetic retinopathy," *Current Diabetes Rep.*, vol. 9, pp. 277–283, Aug. 2009.

[3] K. Guan, C. Hudson, T. Wong, M. Kisilevsky, R. K. Nrusimhadevara, W. C. Lam, M. Mandelcorn, R. G. Devenyi, and J. G. Flanagan, "Retinal hemodynamics in early diabetic macular edema," *Diabetes*, vol. 55, pp. 813–818, Mar. 2006.

[4] A. S. Neubauer, M. Ludtke, C. Haritoglou, S. Priglinger, and A. Kampik, "Retinal vessel analysis reproducibility in assessing cardiovascular disease," *Optometry Vis. Sci.*, vol. 85, p. 247–254, Apr. 2008.

[5] N. Cheung and T. Y. Wong, "The retinal arteriole to venule ratio: Informative or deceptive?" *Graefe's Archive Clinical Experim. Ophthalmol.*, vol. 245, no. 8, pp. 1245–1246, 2007.

[6] G. Liew, P. Mitchell, J. Wang, and T. Wong, "Effect of axial length on retinal vascular network geometry," *Amer. J. Ophthalmol.*, vol. 141, pp. 597–598, Mar. 2006.

[7] S. R. Lesage, T. H. Mosley, T. Y. Wong, M. Szklo, D. Knopman, D. J. Catellier, S. R. Cole, R. Klein, J. Coresh, L. H. Coker, and A. R. Sharrett, "Retinal microvascular abnormalities and cognitive decline: The ARIC 14-year follow-up study," *Neurology*, vol. 73, no. 11, pp. 862–868, 2009.

[8] C. Sun, J. J. Wang, D. A. Mackey, and T. Y. Wong, "Retinal vascular caliber: Systemic, environmental, and genetic associations," *Survey Ophthalmol.*, vol. 54, no. 1, pp. 74–95, 2009.

[9] L. D. Hubbard, R. J. Brothers, W. N. King, L. X. Clegg, R. Klein, L. S. Cooper, A. Sharrett, M. D. Davis, and J. Cai, "Methods for evaluation of retinal microvascular abnormalities associated with hypertension/sclerosis in the atherosclerosis risk in communities study," *Ophthalmology*, vol. 106, pp. 2269–2280, Dec. 1999.

[10] M. D. Knudtson, K. E. Lee, L. D. Hubbard, T. Y. Wong, R. Klein, and B. E. K. Klein, "Revised formulas for summarizing retinal vessel diameters," *Current Eye Res.*, vol. 27, pp. 143–149, Oct. 2003.

[11] M. E. Martinez-Perez, A. D. Hughes, A. V. Stanton, S. A. Thom, N. Chapman, A. A. Bharath, and K. H. Parker, "Retinal vascular tree morphology: A semi-automatic quantification," *IEEE Trans. Biomed. Eng.*, vol. 49, no. 8, pp. 912–917, Aug. 2002.

[12] K. Rothaus, X. Jiang, and P. Rhiem, "Separation of the retinal vascular graph in arteries and veins based upon structural knowledge," *Image Vis. Comput.*, vol. 27, pp. 864–875, Jun. 2009.

[13] E. Grisan and A. Ruggeri, "A divide et impera strategy for automatic classification of retinal vessels into arteries and veins," in *Proc. 25th Annu. Int. Conf. IEEE Eng. Med. Biol. Soc.*, Sep. 2003, pp. 890–893.

[14] S. Vazquez, B. Cancela, N. Barreira, M. Penedo, and M. Saez, "On the automatic computation of the arterio-venous ratio in retinal images: Using minimal paths for the artery/vein classification," in *Proc. Int. Conf. Digital Image Comput., Tech. Appl.*, 2010, pp. 599–604.

[15] H. Li, W. Hsu, M. Lee, and H. Wang, "A piecewise Gaussian model for profiling and differentiating retinal vessels," in *Proc. Int. Conf. Image Process.*, vol. 1. Sep. 2003, pp. 1069–1072.

[16] C. Kondermann, D. Kondermann, and M. Yan, "Blood vessel classification into arteries and veins in retinal images," *Proc. SPIE, Progr. Biomed. Opt. Imag.*, vol. 6512, no. 651247, Feb. 2007.

[17] M. Niemeijer, B. van Ginneken, and M. D. Abramoff, "Automatic classification of retinal vessels into arteries and veins," *Proc. SPIE, Progr. Biomed. Opt. Imag.*, vol. 7260, no. 72601F, Feb. 2009.

[18] R. Estrada, C. Tomasi, M. T. Cabrera, D. K. Wallace, S. F. Freedman, and S. Farsiu, "Exploratory dijkstra forest based automatic vessel segmentation: Applications in video indirect ophthalmoscopy (VIO)," *Biomed. Opt. Exp.*, vol. 3, no. 2, pp. 327–339, 2012.

[19] K. Deng, J. Tian, J. Zheng, X. Zhang, X. Dai, and M. Xu, "Retinal fundus image registration via vascular structure graph matching," *Int. J. Biomed. Imag.*, vol. 2010, no. 906067, Jul. 2010.

[20] R. S. Snell and M. A. Lemp, *Clinical Anatomy of the Eye*. New York, NY, USA: Wiley, 1998.

[21] M. Niemeijer, X. Xu, A. Dumitrescu, P. Gupta, M. A. B. van Ginneken, and J. Folk, "Automated measurement of the arteriolar-to-venular width ratio in digital color fundus photographs," *IEEE Trans. Med. Imag.*, vol. 30, no. 1, pp. 1941–1950, Nov. 2011.

[22] A. Mendonça and A. Campilho, "Segmentation of retinal blood vessels by combining the detection of centerlines and morphological reconstruction," *IEEE Trans. Med. Imag.*, vol. 25, no. 9, pp. 1200–1213, Sep. 2006.

[23] A. Mendonça, B. Dashtbozorg, and A. Campilho, "Segmentation of the vascular network of the retina," in *Image Analysis and Modeling in Opthalmology*, E. Y. K. Ng, U. R. Acharya, J. S. Suri, and A. Campilho, Eds. Boca Raton, FL, USA: CRC Press, 2013.

[24] Z. Guo and R. W. Hall, "Parallel thinning with two-subiteration algorithms," *Commun. ACM*, vol. 2, no. 3, pp. 359–373, 1989.

[25] A. Mendonça, F. Cardoso, A. Sousa, and A. Campilho, "Automatic localization of the optic disc in retinal images based on the entropy of vascular directions," in *Image Analysis and Recognition* (Lecture Notes in Computer Science), vol. 7325. New York, NY, USA: Springer-Verlag, 2012, pp. 424–431.

[26] M. Foracchia, E. Grisan, and A. Ruggeri, "Luminosity and contrast normalization in retinal images," *Med. Image Anal.*, vol. 9, no. 3, pp. 179–190, 2005.

[27] M. Niemeijer, J. Staal, B. Ginneken, M. Loog, and M. Abramoff. (2004). *DRIVE: Digital Retinal Images for Vessel Extraction* [Online]. Available: http://www.isi.uu.nl/Research/Databases/DRIVE

[28] M. Niemeijer, X. Xu, A. Dumitrescu, P. Gupta, B. van Ginneken, J. Folk, and M. Abramoff. (2011). *INSPIRE-AVR: Iowa Normative Set for Processing Images of the REtina-Artery Vein Ratio* [Online]. Available: http://webeye.ophth.uiowa.edu/component/k2/item/270

[29] (2010). *VICAVR: VARPA Images for the Computation of the Arterio/Venular Ratio* [Online]. Available: http://www.varpa.es/vicavr.html

Behdad Dashtbozorg received the B.Sc. degree in electronics from Shahid Beheshti University, Tehran, Iran, in 2006, and the M.Sc. degree in telecommunication systems from Yazd University, Yazd, Iran, in 2009. In July 2010, he joined the Institute for Biomedical Engineering, and has been a Researcher of the Bioimaging Group. Currently, he is pursuing the Ph.D. degree in electrical and computer engineering with the Faculty of Engineering, University of Porto, Porto, Portugal. His current research interests include the advanced image analysis for the assessment of retinal vascular changes.

Ana Maria Mendonça received the Ph.D. degree in electrical engineering from the Faculty of Engineering, University of Porto (FEUP), Porto, Portugal, in 1994. Currently, she is an Associate Professor with the Department of Electrical and Computer Engineering, FEUP. She is the Director of the Master Program in biomedical engineering with the University of Porto. She joined the Institute for Biomedical Engineering (INEB) in 1989, where she is currently a Researcher of the Bioimaging Group. She has been a Board Member with this institute since 2003, where she currently serves as a President of the Board. She served as a Board Member of the Portuguese Association for Pattern Recognition from 2005 to 2012. Her current research interests include image processing and analysis, and more specifically, medical image analysis.

Aurélio Campilho is a Full Professor with the Department of Electrical and Computer Engineering, Faculty of Engineering, University of Porto, Porto, Portugal. From 1994 to 2000, he served as a Chairman of the Institute for Biomedical Engineering (INEB). He served as a President of the Portuguese Association for Pattern Recognition, which is a member of the IAPR. He is the Director of Doctoral Program in electrical and computer engineering with the University of Porto. He is the coordinator of INEB Bioimaging Group. His current research interests include the areas of medical image analysis, image processing, and computer vision. He served as the Organizer of several special issues and conferences. He served as an Associate Editor of the IEEE TRANSACTIONS ON BIOMEDICAL ENGINEERING and the *Machine Vision Applications Journal*. He is a Chairman of the series of conferences ICIAR - International Conference on Image Analysis and Recognition.